



3D-QSAR using ‘Multiconformer’ alignment: The use of HASL in the analysis of 5-HT_{1A} thienopyrimidinone ligands[†]

Salvatore Guccione^{a,*}, Arthur M. Doweyko^b, Hongming Chen^{c,**}, Gloria Uccello Barretta^d & Federica Balzano^d

^aDipartimento di Scienze Farmaceutiche, Università di Catania, viale Andrea Doria 6, Ed. 12, Città Universitaria, I-95125 Catania, Italy; ^bMacromolecular Structure-CADD, Bristol-Myers Squibb, Pharmaceutical Research Institute, P.O. Box 4000, Princeton, NJ 08543, U.S.A.; ^cLaboratory of Computer Chemistry, Institute of Chemical Metallurgy, Chinese Academy of Science, Beijing 100081, P.R. China; ^dCentro CNR di Studio per le Macromolecole Stereordinate ed Otticamente Attive, Università di Pisa, via Risorgimento 35, I-56126 Pisa, Italy

Received 17 November 1999; Accepted 17 April 2000

Key words: HASL, 5-HT_{1A}, multiconformer, receptor modelling, Thienopyrimidinone Ligands (TP)

Summary

The observed 5-HT_{1A} and α_1 -adrenergic receptor (α_1 -AR) receptor binding properties of a series of 23 thienopyrimidinones were used to develop HASL 3D-QSAR models. A single, low energy conformer of the most active analogue in the series, which was consistent with NMR structural studies, was chosen as a template molecule. Alignments of all the molecules to the template were provided by an Amber/MM2 superposition force field. In this manner, each molecule was represented by five separate low energy conformers which were subsequently used in the generation of HASL 3D-QSAR models. Models derived from multiple conformers were found to exhibit enhanced predictivity compared to models based on single, low energy conformers. In addition, the use of contour imaging of HASL multi-conformer model interactions was found to lead to a more consistent interpretation of those molecular features most significant for 5-HT_{1A} receptor binding.

Abbreviations: CoMFA, Comparative Molecular Field Analysis; 2D-NOESY, 2D-Nuclear Overhauser and Exchange Spectroscopy; HASL, Hypothetical Active Site Lattice; HetCor, Heteronuclear Shift Correlation; 5-HT_{1A}, 5-hydroxytryptamine (serotonin) receptor 1A-subtype; OH-DPAT, [³H]-8-hydroxy-2-(di-n-propylamino)tetralin; TP, thienopyrimidinones.

Introduction

Serotonin (Figure 1) modulates many processes in the mammalian peripheral and central nervous system through its interactions with a variety of receptor subtypes, all but one (5-HT₃ subtype) of which are G protein (heterotrimeric GTP-binding protein)-coupled

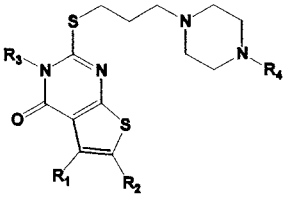
[1, 2]. The critical molecular features of serotonin (indole ring and alkylamino side chain) and details of 5-HT functional and structural similarity to other receptors is well documented [3–7]. Although the precise function of the 5-HT receptors remains undefined, direct interactions with the 5-HT_{1A} receptor via selective ligands (agonists or antagonists) may have beneficial effects in a large number of diseases comprehensive of a number of neuropsychiatric disorders (anxiety and depression) [8, 9]. To date, 3D-QSAR methodology applied to the 5-HT_{1A} receptor has been largely limited to CoMFA analyses applied across a variety of chemotypes [10–12].

[†]Paper in part presented at the 12th European Symposium on Quantitative Structure-Activity Relationships, Molecular Modelling and Prediction of Bioactivity, Copenhagen, Denmark, August 23–28, 1998.

*To whom correspondence should be addressed. E-mail: guccione@mbox.unict.it

**Present address: Bayer AG, Pharma-Forschung, PH-R Struktur-forschung, D-42096 Wuppertal, Germany.

Table 1. Thienopyrimidinones. Structures and observed 5-HT_{1A} and α_1 binding

							
	R1	R2	R3	R4	HT pIC50	Alpha pIC50	Diff pIC50
1	Me	Me	H	2-CIPhenyl	6.34	6.79	-0.45
2	Me	Me	H	3-CIPhenyl	6.01	6.52	-0.51
3	Me	Me	H	2-OMePhenyl	7.62	7.40	0.22
4	Me	Me	H	1-Naphtyl	6.45	6.05	0.40
5	Me	Me	H	2-Pyrimidyl	6.65	5.96	0.69
6	-(CH ₂) ₄ -		H	2-CIPhenyl	6.03	6.78	0.75
7	-(CH ₂) ₄ -		H	2-OMePhenyl	7.23	7.42	-0.19
8	-(CH ₂) ₄ -		H	1-Naphthyl	6.43	6.35	0.08
9	-(CH ₂) ₄ -		H	2-Pyrimidyl	6.30	5.74	0.56
10	H	Ph	H	2-OMePhenyl	6.41	6.65	-0.24
11	H	Ph	H	1-Naphthyl	5.70	5.61	0.09
12	-(CH=CH)-		H	2-OMePhenyl	7.34	7.04	0.30
13	H	H	NH ₂	2-OMePhenyl	8.92	8.54	0.38
14	-(CH ₂) ₄ -		Me	2-OMePhenyl	8.15	7.19	0.96
15	-(CH ₂) ₄ -		NH ₂	2-OMePhenyl	8.89	7.41	1.48
16	Me	Me	NH ₂	Phenyl	8.48	7.37	1.11
17	Me	Me	Me	2-OMePhenyl	8.52	7.57	0.95
18	Me	Me	NHPhenyl	2-OMePhenyl	6.30	7.49	-1.19
19	Me	Me	Me	2-Pyrimidyl	7.19	5.69	1.50
20	Me	Me	NH ₂	2-Pyrimidyl	8.17	6.30	1.87
21					9.10	7.44	1.66
22					9.30	8.40	0.90
23	Me	Me	NH ₂	2-OMePhenyl	9.52	8.14	1.38

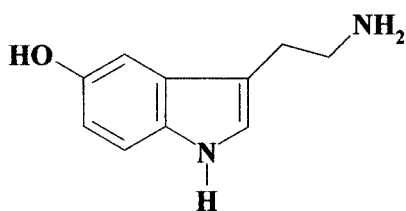


Figure 1. 5-HT (serotonin) structure.

The thienopyrimidinone chemotype (Table 1) represents a group of semirigid 5-HT_{1A} ligands with which to study the effects of different substituents on 5-HT receptor binding, since as a class, they fit the structural requirements for recognition at serotonin receptors and have the added benefit of being rela-

tively easy to synthesize and modify. The 3-carbon side chain, acting as a spacer between the heterocyclic scaffold and the pharmacophoric arylpiperazine moiety was found to be a substantial structural prerequisite in this class of compounds for optimal 5-HT_{1A} affinity and selectivity [13, 14].

The goal of the present study was to use a 3D-QSAR technique, HASL [15–19], to develop predictive models from a homologous series which would have the potential to include SARs within different classes of agonists and antagonists at 5-HT_{1A} receptors. The analysis of these semi-rigid 5-HT_{1A} thienopyrimidinone ligands would permit the identification of substructures correlated to 5-HT_{1A} and α_1 -AR selectivity [13, 14]. Differences in pIC₅₀ (5-

HT_{1A}- α_1 -AR) were also analyzed in an attempt to define those features most critical to the design of selective, high affinity 5-HT_{1A}- and α_1 -ligands. In addition, it was of interest to determine if the use of multiple conformers could provide enhanced model predictivity and substructure mapping of those molecular properties most significant to binding.

Materials and methods

Receptor binding assays

5-HT_{1A} and α_1 -AR receptor binding assays were performed as described previously [13, 14]. Dose inhibition curves were analyzed by the 'Allfit' program to obtain the concentration of unlabeled drugs that inhibited ligand binding by 50% [13]. The affinities of reference compounds were used as controls. It should be noted that no distinction was made between agonists or antagonists since this information was not available [13, 14]. The [[(arylpiperazinyl)alkyl]thio] thieno-[2,3-d]pyrimidinones (**1–23**) investigated in this study are listed in Table 1, along with both the 5-HT_{1A} and α_1 -AR binding data. The activities used in the HASL analyses of training and test sets are expressed as pIC₅₀ ($-\log$ IC₅₀), where IC₅₀ is the concentration of unlabeled ligand that causes 50% displacement of ³HDPAT for HT_{1A} or [³H]prazosin for α_1 receptor, respectively.

NMR conformational analysis

NMR measurements were performed on a Varian VXR-300 spectrometer equipped with a temperature control unit ($\pm 0.1^\circ\text{C}$). ¹H and ¹³C characterization were performed at 300 MHz and 75 MHz, respectively, in CDCl₃ at 25 °C. The 2D NMR spectra were obtained by using standard sequences. The 2D NOESY spectra were acquired with a spectral width of 2200 Hz in 2K data points using 8 scans for each of the 512 t₁ increments, with a mixing time of 600 ms and a relaxation delay of 5 s. A Gaussian function was applied for processing in both dimensions. The HETCOR spectra were acquired with a spectral width of 13 000 Hz in F₂ and 2200 Hz in F₁ in 2K data points using 64 scans of the 512 increments. The relaxation delay was 5 s. The data were zero-filled to 2K \times 1K and a Gaussian function was applied for processing in both dimensions. The ¹³C spin-lattice relaxation times were measured by the inversion-recovery method.



Figure 2. Traces of the 2D NOESY map (300 MHz, CDCl₃, 25 °C, $\tau_m = 0.6$ s) of **23** corresponding to: (a) OMe protons, (b) piperazine methylene protons H_e, (c) piperazine methylene protons H_d.

Molecular modeling

The molecular modeling studies were performed using the following software: SPARTAN (Version 5.03) [20], SYBYL (Versions 6.3 and 6.5), HASL (PC Version 3.30, UNIX Version 4.00S (Sybyl Module) [19] and a UNIX version written specifically for multiconformer analysis), and FLO96/QXP [21, 22] as configured on an SGI R10000 and a R5000 workstations operating under IRIX 6.4 and 6.3, respectively.

The optimized structure of the most active analogue, compound **23**, was used as the building block for all the other structures which were in turn re-optimized prior to QSAR analysis. Molecules were built using the fragment library within SPARTAN 5.03. SPARTAN *spinput* files were ported to SYBYL (Versions 6.3 and 6.5) as mol2 files. In order to determine the lowest energy conformation, i.e., geometries close to (global and local) energy minima, a systematic conformational search on compound **23** was carried out by molecular mechanics using the conformational search module within SYBYL 6.3 and 6.5 [23]. Energy minimization by molecular mechanics



Figure 3. Conformation of compound **23** used as a template target (thick bonds) shown with 5 conformers of each of 23 molecules (thin bonds).

was performed with the TRIPOS force field. Following the conformational search, the structure of the lowest energy conformer was minimized using the standard TRIPOS force field and the Powell minimizer (MAXIMIN 2 sub-routine) with the electrostatic contribution. All other settings were taken with default values. The torsion ranges on the alkyl chain between the thienopyrimidine ring and the piperazine (C–S–C–C–C–N) ring were scanned within 0–360° (10° increments). All structures were fully optimized using the PM3 option as implemented in MOPAC [23]. All molecules were aligned on compound **23**. In the present investigation, FLO96/QXP was used to flexibly dock each molecule to the template structure through 20 Monte Carlo rotational randomization cycles, retaining 5 best fit superposed rotamers per molecule. In this way, a total of 115 rotamers were obtained and used in the 3D-QSAR HASL analyses. Each conformer is the result of fitting the Monte Carlo-generated sibling to the common template molecule, resulting in a conformer population reflecting the constraints of the model. It is reasoned that the most populated conformer space should have the most significant effect in the model creation. 3D-QSAR analyses were conducted by applying HASL in two ways: (1) using the best single low energy conformer obtained for each molecule and (2) using all five conformers as obtained by the FLO96/QXP-mediated conformational mapping.

HASL computation was implemented on SGI O2 R5000 (IRIX 6.3) and SGI R10000 (IRIX 6.4) workstations. Default atom types were used (H = -1, 0, +1) and the lattice grid spacing was 1.5 Å. Models were

Table 2. ¹H NMR (300 MHz, CDCl₃, 25 °C) chemical shifts (δ, ppm) of **17**, **18** and **23**

Protons	17	18	23
H _a	3.24	3.13	3.13
H _b	1.94	1.94	1.94
H _c	2.52	2.52	2.53
H _d	2.64	2.64	2.65
H _e	3.08	3.08	3.08
Me	2.40	2.35	2.40
Me	2.30	2.32	2.31
OMe	3.82	3.84	3.83
Ar	6.77–7.00	6.61–7.78	6.79–7.01
NH ₂	–	–	4.76
NH	–	6.93	–
NMe	3.49	–	–

iteratively solved to an average error in prediction of 0.001 log units activity. Using the full 23 compound data set, three HASL models were developed: 5-HT_{1A}, α₁-AR, and the difference data in each case yielding models containing 427 lattice points. Both the single and multiconformer HASL-derived 3D pharmacophoric models were subjected to leave-one-out cross-validation analysis wherein the activity of each compound was predicted by a model based on the remaining structures.

Results and discussion

Template molecule

Compounds **17**, **18**, and **23** were characterized by 2D NOESY and HETCOR analyses (Tables 2 and 3). Their conformations were determined by analyzing the intermolecular dipolar interactions by means of 2D NOESY spectroscopy. In the case of compound **23**, the methylene protons, belonging to the piperazine moiety, originate NOEs on the aromatic protons of the *o*-methoxyphenyl substituent and on the methylene chain (traces b and c, Figure 2). Moreover, methoxy protons produce NOEs only on the aromatic proton adjacent to them (trace a, Figure 2) and no dipolar

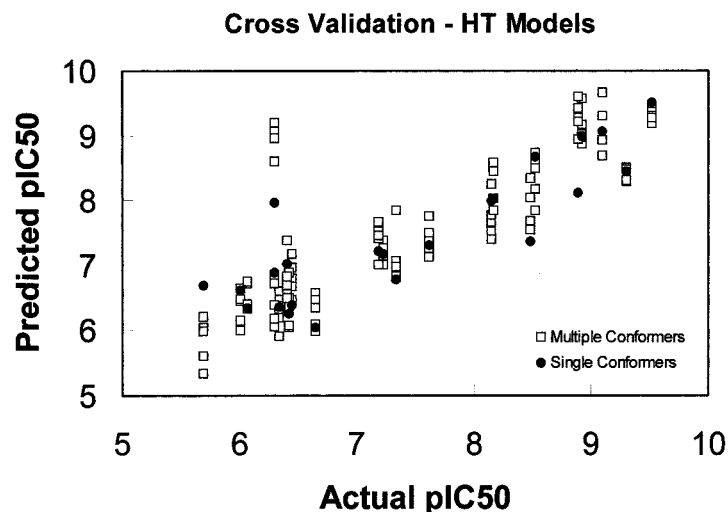


Figure 4. Cross-validation results for HASL HT models: single conformer (black circles) $r^2(\text{cv}) = 0.746$ (0.830); multiple conformers (white squares) $r^2(\text{cv}) = 0.677$ (0.868); averaged multiple conformers $r^2(\text{cv}) = 0.715$ (0.919); values in parentheses are for 22 molecules, excluding compound **18** (grey squares).

Table 3. ^{13}C NMR (75 MHz, CDCl_3 , 25 °C) chemical shifts (δ , ppm) of **17**, **18** and **23**

Carbons	17	18	23
Me	12.9, 13.0	12.8, 12.9	12.8, 12.9
a	30.1	29.2	29.2
b	26.1	26.1	26.1
c	57.2	57.3	57.4
d	53.3	53.3	53.3
e	50.6	50.6	50.6
OMe	55.3	55.3	55.3
NMe	29.7	—	—
Ar	111.2, 118.2, 120.9, 122.8	111.2, 114.3, 118.2, 120.9, 122.8, 122.8, 129.3	111.2, 118.2, 120.9, 122.8
Quaternary	119.1, 127.7, 129.1, 141.3, 152.2, 156.5, 158.8, 161.3	119.8, 128.4, 128.7, 129.3, 141.4, 145.1, 152.3, 157.7, 159.8, 161.7	118.8, 128.4, 128.7, 141.4, 152.2, 157.9, 158.3, 161.5

interaction is originated by NH_2 or methyl protons. Therefore, compound **23** assumes a conformation in which the chain linked to the sulfur atom is in a zig-zag planar arrangement, bringing the piperazine and aromatic rings far away from the thienopyrimidinone moiety. The two substituents linked to the two nitrogens of the piperazine ring mainly assume a

pseudoequatorial arrangement which effectively prevents any significant spatial proximity between the aromatic protons of the methoxyphenyl substituent at one nitrogen of the piperazine ring and the piperazine methylene directly linked to the other nitrogen. The aromatic moiety is mainly perpendicular to the plane of the piperazine ring and the methylene protons directly linked to the sulfur atom are far away from the amino group. The ^{13}C longitudinal relaxation times (T_1), determined for piperazine and chain methylene carbons, are both 0.46 s and those of the aromatic methines are 0.76 s, according to a rigid structure tumbling isotropically. Analogous NOESY analyses and ^{13}C relaxation time determinations have also been carried out on other related less active compounds, i.e., **17** and **18**. Their stereochemical and dynamic features are similar to those already discussed for **23** and no information on the relationship between conformation and activity was found. The conformation of the template molecule **23** was based on these findings, as well as molecular mechanics analyses discussed previously, and is illustrated in Figure 3 along with 115 FLO96/QXP fitted conformers. The piperazine ring is perpendicular to the aromatic moiety (free electron lone pair of the basic nitrogen parallel to the plane of the aromatic moiety) and the alkyl side chain is in an extended form (linear alkyl chain). Although ab initio calculations routinely favor a planar orientation for the aromatic moiety to the piperazine ring (conjugation of the nitrogen lone pair to the π -electron

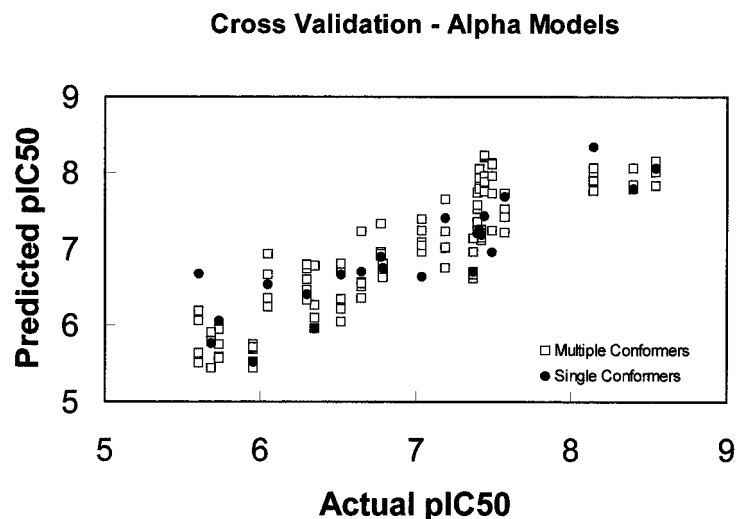


Figure 5. Cross-validation results for HASL Alpha models: single conformer (black circles) $r^2(\text{cv}) = 0.775$ (0.786); multiple conformers (white squares) $r^2(\text{cv}) = 0.797$ (0.804); averaged multiple conformers $r^2(\text{cv}) = 0.852$ (0.858); values in parentheses are for 22 molecules, excluding compound **18** (grey squares).

system), the molecular mechanics derived orientations were used throughout this investigation for reasons of overall consistency and ease of use.

Conformation generation

A number of approaches have been described in the literature to estimate conformations under conditions which are relevant for structure-activity relationship studies [24]. The final geometries can provide an orientation rule for ligands that enables the use of 3D-QSAR methods. The success of the analysis does not depend on the method itself but the way the molecules are aligned in order to reproduce the receptor-bound motif. Besides the well known and widely applied Active Analog approach [25] and the Field Fit Method [26], approaches to solve this problem have been recently described [27–29]; furthermore, automated tools [30–32] of which DISCO [33] is the most representative have also been developed. In addition, COMPASS, an automated binding site modeling tool utilizing multiple molecular poses and a neural net has shown promise in identifying potential submolecular interaction sites [34]. FLO96/QXP (Flo) is a recently developed ‘multifunctional’ molecular design program which uses an Amber/MM2 force field implemented to provide attractive energetics for atoms of the same type, while minimizing individual internal energies to flexibly align molecules upon a template target (which is held rigid) with the objective of maximizing the superpositioning of similar atom types

through the use of a superposition force field. Superposition energy scores and internal molecular energies are co-minimized to yield a series of overlapped structures with low internal energies. A single molecule or a selected subset of such co-minimized structures can be used as a fixed pharmacophore, so that other molecules can be flexibly fitted and minimized to the model.

HASL analyses

The 3D-QSAR HASL models based on 23 thienopyrimidinones were found to be highly predictive for both 5-HT_{1A} and α_1 -AR binding. Cross-validation (leave-one-out) analyses were conducted for three binding end points: HT, α_1 -AR and Diff (HT- α_1 -AR), and the results of these analyses are shown in Table 4, and illustrated in Figures 4–6. Using the cross-validation correlation coefficient (r^2_{cv} , q^2) [35] as a reflection of predictivity, both HT_{1A} and Alpha models performed very well. As compound **18** is problematic in this series, since it is the only congener having a bulky phenyl moiety at R3, predictivity (r^2_{cv} , q^2) [35] was also computed for the other 22 compounds to avoid the significant perturbation of this outlier. It must be noted that the outlier **18** is the only compound showing a reasonable and quite selective α_1 -AR activity, suggesting more tolerance for bulky groups at the α_1 -adrenergic receptors (α_1 -AR) whereas the 5-HT_{1A} receptor appears to exhibit tighter steric requirements. On the other hand, it may be spec-

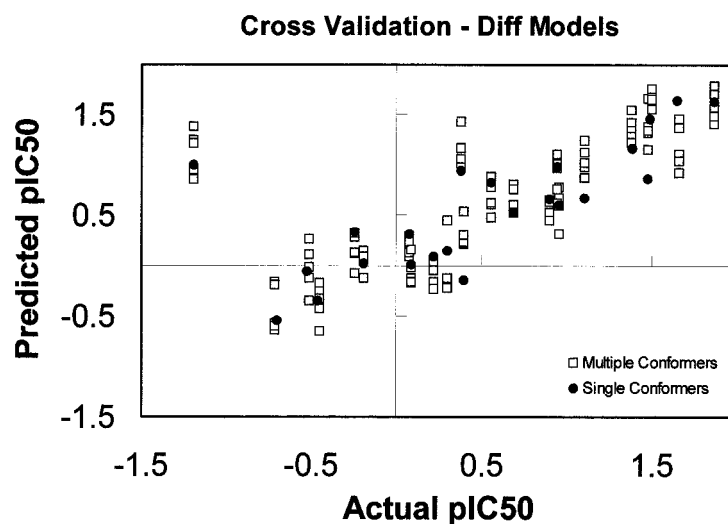


Figure 6. Cross-validation results for HASL Diff models (HT-Alpha): single conformer (black circles) $r^2(\text{cv}) = 0.525$ (0.811); multiple conformers (white squares) $r^2(\text{cv}) = 0.488$ (0.786); averaged multiple conformers $r^2(\text{cv}) = 0.516$ (0.830); values in parentheses are for 22 molecules, excluding compound **18** (grey squares).

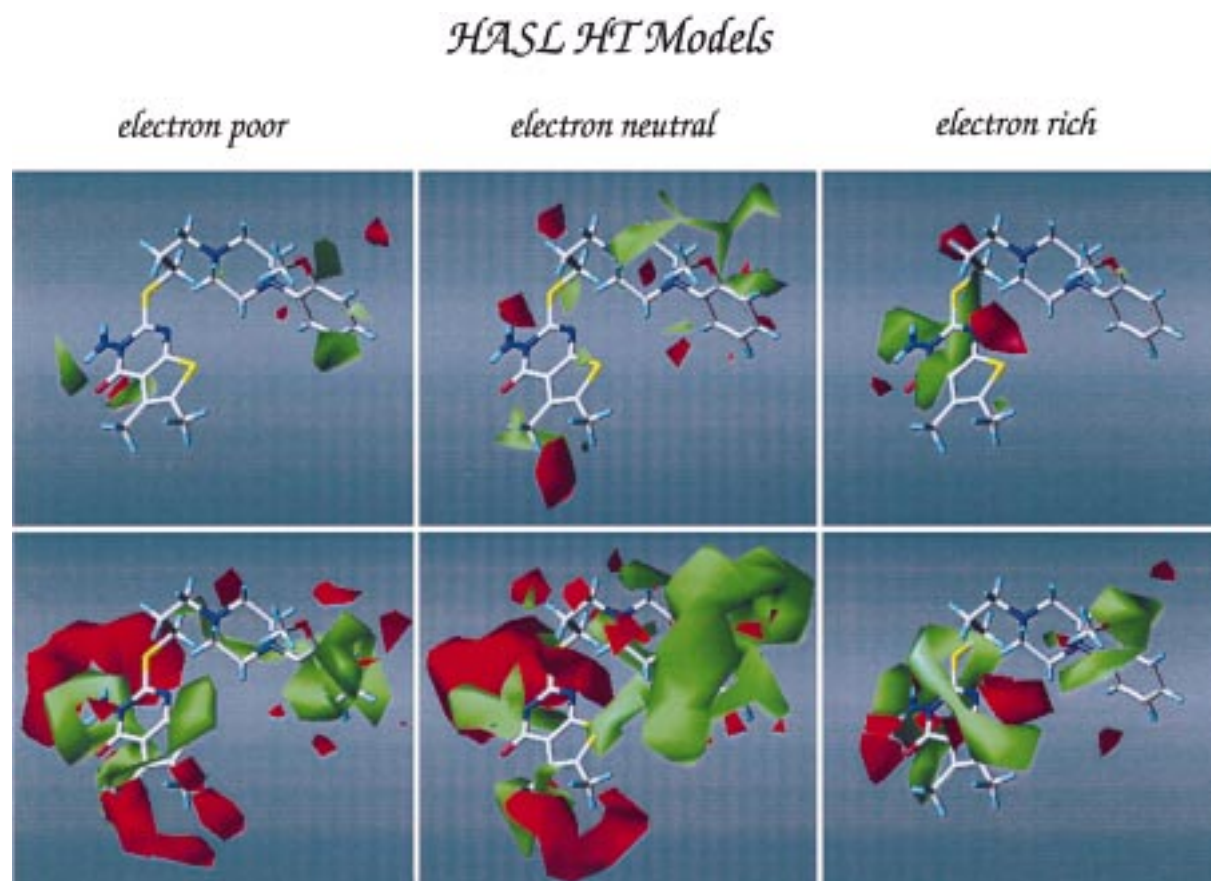


Figure 7. HASL HT contour maps: Positive effect on binding illustrated as a green contour at partial $\text{pIC}_{50} = 0.09$; negative effect on binding illustrated as a red contour at partial $\text{pIC}_{50} = -0.01$. Single conformer model in upper row, multiple conformer model in lower row.

HASL Alpha Models

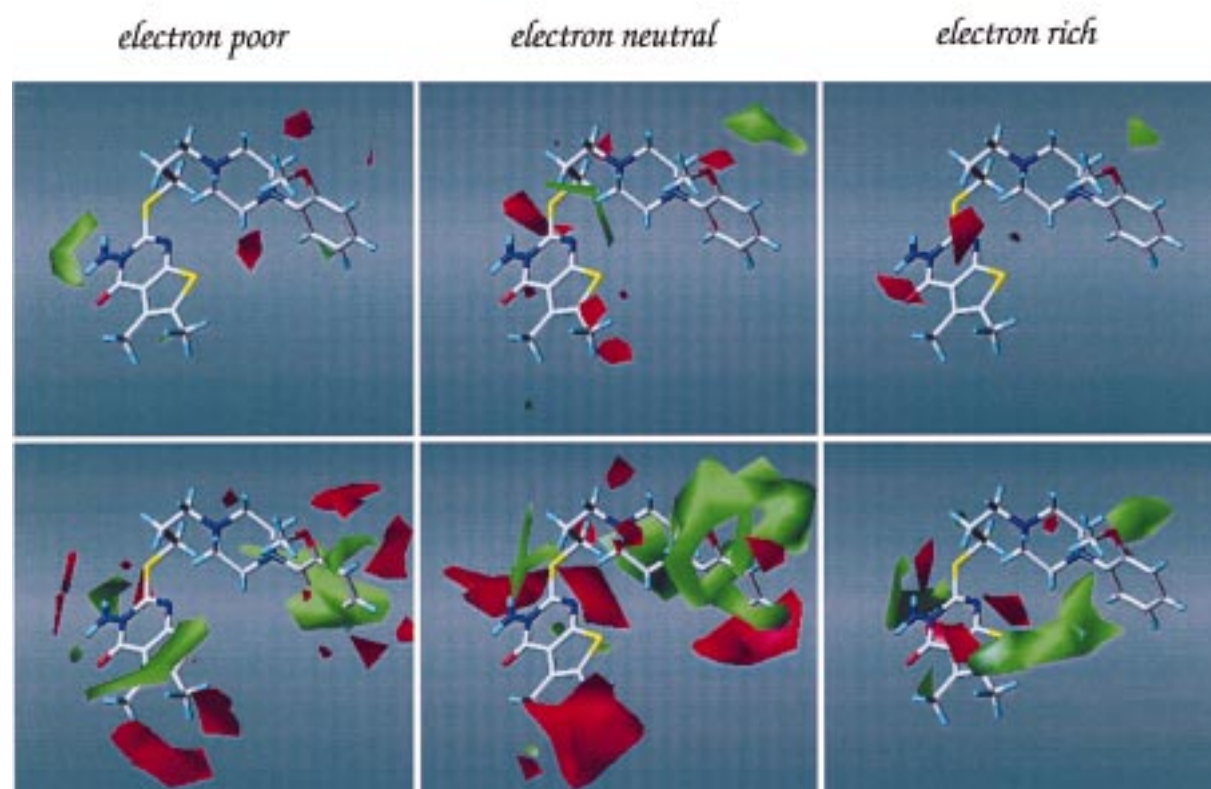


Figure 8. HASL Alpha contour maps: Positive effect on binding illustrated as a green contour at partial $\text{pIC}_{50} = 0.09$; negative effect on binding illustrated as a red contour at partial $\text{pIC}_{50} = -0.01$. Single conformer model in upper row, multiple conformer model in lower row.

Table 4. Cross-validated HASL model results

	HT (5-HT _{1A})	Alpha (α_1)	Diff (HT - Alpha)
r_{cv}^2 (single conformer)	0.746 (0.830) ^a	0.775 (0.786)	0.525 (0.811)
r_{cv}^2 (multiple conformers)	0.677 (0.868)	0.797 (0.804)	0.488 (0.786)
r_{cv}^2 (averaged multiple conformers)	0.715 (0.919)	0.852 (0.858)	0.516 (0.830)

^aValues in parentheses were determined for 22 compounds, excluding compound **18**.

ulated that the negative effect of including compound **18** in the HASL calculation regarding the α_1 -AR might be due to a different alignment. The antagonist-receptor binding interactions are likely to be different for each compound at the G-protein coupled receptors even for closely related members of chemical series [36]. When comparing (r_{cv}^2 , q^2) [35] values, it was of interest to note that any increase in predictivity in the multiple conformer models was masked by the increase in the number of points for the multiple conformer cases, prompting a closer look at the aver-

aged predictions. In both HT and α_1 -AR models the averaged multiple conformer predictions represented an improvement over the single conformer options: $r_{cv}^2(q^2) = 0.919$ versus 0.830 (HT) and $r_{cv}^2(q^2) = 0.858$ versus 0.786 (α_1 -AR). In addition, although the Diff model (HT- α_1 -AR) showed some slight improvement as well ($r_{cv}^2(q^2) = 0.830$ versus 0.811), such a conclusion should be considered tenuous as the difference data only spanned about two orders of magnitude and are therefore subject to artifactual correlations.

HASL Diff Models

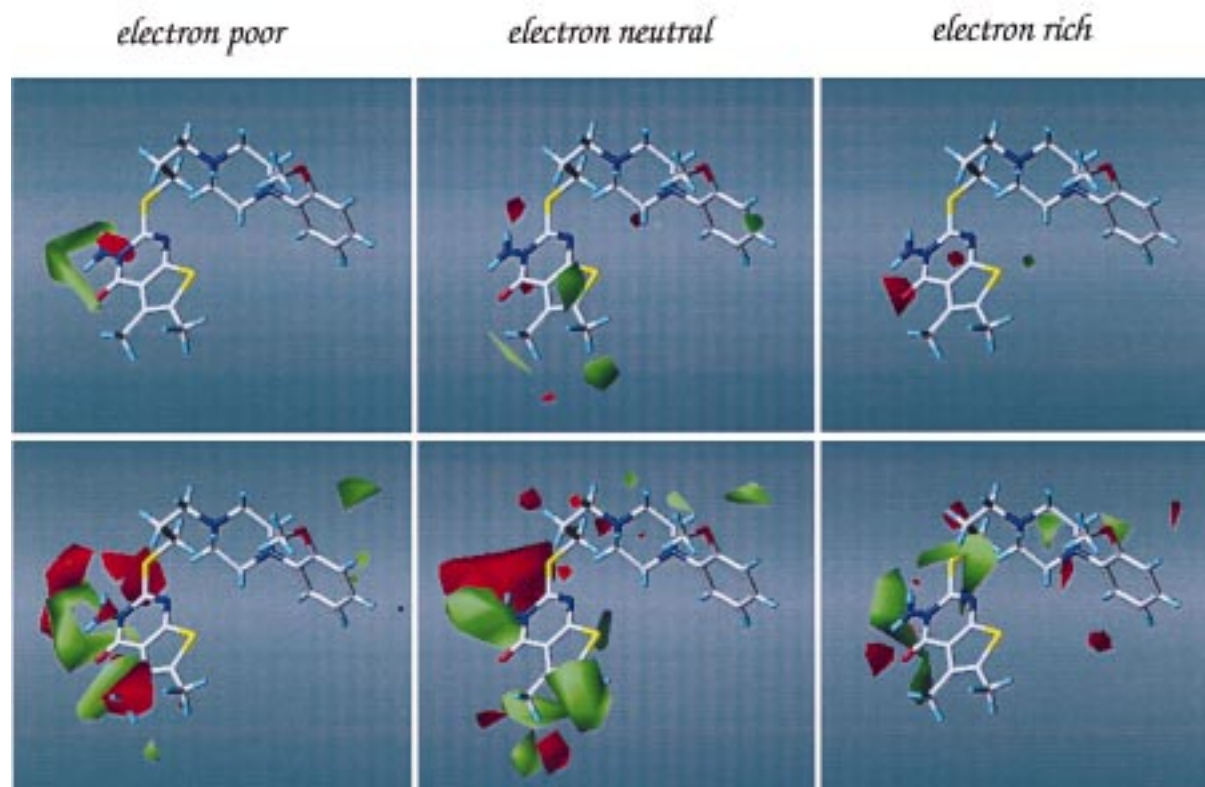


Figure 9. HASL Difference (HT-Alpha) contour maps: Positive effect on binding illustrated as a green contour at partial $\text{pIC}_{50} = 0.05$; negative effect on binding illustrated as a red contour at partial $\text{pIC}_{50} = -0.05$. Single conformer model in upper row, multiple conformer model in lower row.

Single and multiple conformer 3D-QSAR HASL models were developed using the full set of 23 compounds. The calculated partial pIC_{50} values (those occurring at the HASL lattice points reflecting specific atom type correlations) were contoured at similar levels (to reflect the effects of substructure binding of three atom types: electron-rich (O, N, F, Cl, Br, I and S), electron-poor (carbonyl C, hydrogens in OH, NH, COOH, and =CH), and electron-neutral (C, H). These contours are illustrated in Figures 7–9 and are color coded green for positive contributions to binding affinity (0.05 to 0.09 partial pIC_{50} units) and red for negative contributions (–0.01 to –0.05 partial pIC_{50} units). It was found that these contours were more contiguous and interpretable for the multiple conformer HT models (Figure 7) and illustrate that binding activity is increased when (1) electron-neutral (steric) atom types are introduced at R4, (2) a combination of electron-rich and -poor atom types are located at

R3, and (3) an electron-rich ortho phenyl substituent exists at R4 (e.g., 2-MeOPhenyl). HT_{1A}-binding is decreased when large electron-neutral (or electron-poor) groups occupy R3 (as evidenced by the phenyl group in compound **18**). In the case of α_1 -AR models (Figure 8), binding is predicted to be enhanced by the same effects observed for HT (1–3) except for compound **18** as indicated above. Interestingly, only a relatively minor negative effect is observed for large R3 groups, while steric interactions (electron-neutral) at the R2 position appear to be significantly correlated with a decrease in binding activity (also observed for electron-neutral groups in the HT model). The Diff models (HT- α_1 -AR, Figure 9) reflect the overall trends observed above and appear to point to good binding affinity (enhanced HT binding over alpha) when R3 is occupied by small combinations of electron-rich and -poor atom types (e.g. NH₂) and R2 is occupied by electron-neutral (steric) groups.

In addition to the interpretive strengths of a 3D-QSAR HASL multi-conformer model, it is also evident that the resulting contours are smoothed out compared to those arising from the single conformer option. For example, in the single conformer HT model, the R4 positive steric effect (green) is displayed as a broken feature while the multiple-conformer model yields a clear contiguous contour (Figure 7). In the same model, the large negative effect of steric bulk at R3 (red) is enhanced for the multi-conformer case, and only appears as one of many possibilities in the single conformer case. The appearance of discrete, isolated contours derived from single conformers is clearly evident, while contours obtained from multiple conformers tend to cover more space in an unbroken manner. In some instances, the single conformer model may be reflecting an edge effect in alignment, which highlights an artifactual interaction present only because similar atoms were not completely superposed. These types of alignment problems are typical in the course of building 3D-QSAR models, and appear to be at least somewhat ameliorated when using multiple conformers. These conclusions are not unique to the HASL methodology, as similar results (unpublished data) were obtained using CoMFA [23] and PARM (Pseudo Atomic Receptor Model) [14]. Thus, it is expected that the advantages of multiple conformer use can be generalized to other 3D-QSAR approaches, particularly those sensitive to the selection of an alignment paradigm.

Conclusions

Multiconformer 3D-QSAR (HASL) was demonstrated to yield robust cross-validated models for the 23 thienopyrimidinones which were more predictive than models based on single conformers. By applying a combination of techniques, namely, conformer generation and superpositioning (FLO96/QXP) and 3D-QSAR (HASL), the resulting models were found to be predictive, and effectively mapped substructural space in a way which was consistent with, and quantified to, known SAR for the series. Furthermore, as the alignment problems typical to 3D-QSAR analyses were avoided by averaging conformer occupation within designated constraints, this technique may represent an advancement over other alignment-based methods in avoiding artifactual edge effects and providing smooth interaction contours amenable to direct interpretation.

Acknowledgements

The authors thank Dr Colin McMartin for making available the FLO software. S.G. thanks TRIPOS Inc. for computational facilities (SYBYL Molecular Modelling Software version 6.5). This study was supported by MURST (Italy) for the scientific program in CO7X Field (1997-1999): 'Synthesis of Ligands to Serotonergic Receptors'.

References

1. Zifa, E. and Fillion, G., *Pharmacol. Rev.*, 44 (1992) 401.
2. Data from Trends in Pharmacological Sciences Receptor Nomenclature Supplement (1996).
3. England, L.J., Imperial, J., Jacobsen, R., Craig, A.G., Gulyas, J., Akhtar, M., Rivier, J., Julius, D. and Olivera, B.M., *Science*, 281 (1998) 575.
4. Agarwal, A., Pearson, P.P., Taylor, E.W., Li, H.B., Dahlgren, T., Herslöf, M., Yang, Y., Lambert, G., Nelson, D.L., Regan, J.W. and Martin, A.R., *J. Med. Chem.*, 36 (1993) 4006.
5. Fargin, A., Raymond, J.R., Lohse, M.J., Kobilka, B.K., Caron, M.G. and Lefkowitz, R.J., *Nature*, 335 (1988) 358.
6. Hoflack, J., Trumpp-Kallmeyer, S. and Hilbert, M.F., In Kubinyi, H. (Ed.), *3D QSAR in Drug Design. Theory Methods and Applications*, ESCOM, Leiden, 1993, pp. 355-372.
7. Kuipers, W., van Wijngarden, I. and IJzerman, A.P., *Drug. Des. Discov.*, 11 (1994) 231.
8. Broekkamp, C.L., Leysen, D., Peeters, B.W. and Pinder, R.M., *J. Med. Chem.*, 38 (1995) 4615.
9. Blier, P. and de Montigny C., *Trends Pharmacol. Sci.*, 15 (1994) 220.
10. Gaillard, P., Carrupt, P.-A., Test, B. and Schambel, P., *J. Med. Chem.*, 39 (1996) 126.
11. Cox, A.G., Taylor, E.W., Agarwal, A., Li, H.B., Yang, Y. and Martin, A.R., Book of Abstracts, 210th ACS National Meeting, Chicago, IL, August 20-24 (1995).
12. Agarwal, A., Pearson, P.P., Taylor, E.W., Li, H.B., Dahlgren, T., Herslof, M., Yang, Y., Lambert, G., Nelson, D. et al., *J. Med. Chem.*, 36 (1993) 4006.
13. Modica, M., Santagati, M., Russo, F., Parotti, L., De Gioia, L., Selvaggini, C., Salmona, M. and Mennini, T., *J. Med. Chem.*, 40 (1997) 574.
14. Santagati, M., Doweiko, A., Santagati, A., Modica, M., Gucione, S., Chen, H.M., Uccello Barretta, G. and Balzano, F., In Gundertofte, K. and Jorgensen, F.S. (Eds), *Molecular Modelling and Prediction of Bioactivity-Proceedings of the 12th European Symposium on Quantitative Structure-Activity Relationships-Copenhagen, Denmark, August 23-28, 1998*, Plenum Publishing Corporation, 1999, pp. 185-196.
15. Doweiko, A.M., *J. Med. Chem.*, 31 (1988) 1396.
16. Doweiko, A.M., *J. Med. Chem.*, 37 (1994) 1769.
17. Kaminski, J.J. and Doweiko, A.M., *J. Med. Chem.*, 40 (1997) 427.
18. Doweiko, A.M. and Avery, M.A., *J. Comput.-Aided Mol. Design*, 12 (1998) 165.
19. a. HASL 3.30 (pc) and source code for UNIX is available from Hypothesis Software, Long Valley, NJ, USA.
b. The Sybyl-interfaced version of HASL (Version 4.00S for SGI platforms) is available from eduSoft, LC, P.O. Box 1811,

- Richmond, VA 23005, USA and has several innovative features that take unique advantage of the power of Sybyl to create HASL models and graphically examine the model results. It includes an expanded parameter set that allows two values per atom type, a new cross-validation routine, interfaces to HINT and Molconn-Z, and new map contouring algorithms that provide a novel and informative view of the HASL model results.
20. SPARTAN version 5.0.3., Wavefunction, Inc., Irvine, CA, USA.
 21. McMartin, C. and Bohacek, R.S., *J. Comput.-Aided Mol. Design*, 11 (1997) 333.
 22. QXP is the molecular mechanics module in FLO96, a molecular design program commercially available from Colin McMartin, Thistlesoft, P.O. Box 227, Colebrook, CT 06021, USA.
 23. SYBYL Molecular Modelling Software version 6.3 and 6.5, Tripos Inc., St. Louis, MO, USA.
 24. Hopfinger, A.J., Wang, S., Tokarski, J.S., Baiqiang, J., Albuquerque, M., Madhav, M., Prakash, J. and Duraiswami, C., *J. Am. Chem. Soc.*, 119 (1997) 10509.
 25. Dammkoehler, R.A., Karasek, S.F., Shands, E.F.B. and Marshall, G.R., *J. Comput.-Aided Mol. Design*, 3 (1989) 3.
 26. a. Clark, M., Cramer III, R.D., Jones, D.M., Patterson, D.E. and Simeroth, P.E., *Tetrahedron Comput. Methodol.*, 3 (1990) 47.
b. Smith, G., SEA: Steric and Electrostatic Alignment Molecular Superposition Program; QCPE Program No. 567; Department of Chemistry, Indiana University, Bloomington, IN, USA.
 27. Nicklaus, M.C., Shaomeng, W., Driscoll, J.S. and Milne, W.A., *Bioorg. Med. Chem.*, 3 (1995) 411.
 28. Allen, F.H., In Domenicano, A. and Hargittai, I. (Eds), *Accurate Molecular Structures*, Oxford University Press, Oxford, 1992, p. 355.
 29. Langer, T. and Hoffmann, R.D., *J. Chem. Inf. Comput. Sci.*, 38 (1998) 325.
 30. Lemmen, C., Hiller, C. and Lengauer, T., *J. Comput.-Aided Mol. Design*, 12 (1998) 491.
 31. Klebe, G., Mietzner, T. and Weber, F., *J. Comput.-Aided Mol. Design*, 13 (1999) 35.
 32. Kazuhiko, I. and Shuichi, H., *J. Comput.-Aided Mol. Design*, 13 (1999) 499.
 33. Martin, Y.C., Bures, M.G., Danaher, E.A., DeLazzer, J., Lico, I. and Pavlik, A.J., *J. Comput.-Aided Mol. Design*, 7 (1993) 83.
 34. Jain, A.N., Harris, N.L. and Park, J.Y., *J. Med. Chem.*, 38 (1995) 1295.
 35. Baroni, M., Costantino, G., Riganelli, D., Valigi, R. and Clementi, S., *Quant. Struct.-Act. Relat.*, 12 (1993) 9.
 36. Santagati, A., Longmore, J., Guccione, S., Langer, T., Tonnel, E., Modica, M., Santagati, M., Monsù Scolaro, L. and Russo, F., *Eur. J. Med. Chem.*, 32 (1997) 973.